Geological Study on Uraniferous Pegmatitic Veins and Late Quartz Stockworks Hosted by Alkali Syenite Batholith, Miri Barra, Nuba Mountains Sudan

BADR EL DIN KHALIL AHMED & ABDEL RAHMAN KHIDER HASSAN

University of Khartoum

A follow-up prospecting was executed to investigate a gamma-ray anomaly in the Miri area in the southern part of the Nuba Mountains, Sudan. An overview of the geology, radiometry and geochemistry involved is presented.

The anomaly is related to structurally controlled uraniferous pegmatitic veins and quartz-rich stockworks genetically related to alkali syenite batholith, and is principally raised by uranium and thorium at high Th/U ratio over a local background of approximately 90 cps and a regional background of 50 cps. In addition to uranium and thorium, there is a variety of incompatible trace elements: Nb, Ta, Zr, Ni, Ba, Be, Sr, Y, Ce, La, and Rb. The elemental distribution in the analyzed samples is erratic and displays variable abundances. Constrains on geochemistry of the mineralizing solutions are reviewed on the basis of mineralogical investigations and geostatistical interpretation of geochemical data.

Mineralization is interpreted to be related to pegmatitic melts and late-stage hydrothermal solutions, suggesting multiphase emplacement.

The geological investigations which have covered the area up to now are inadequate to reveal the feasible economic potentialities of U-Th mineralization; detailed and costly explorational work is still needed. However, the environmental impact of mineralization, due to U and Th and their radiogenic daughter products, is observed and should be studied in detail.

Key words: geological study, uraniferous pegmatitic veins, guartz stockworks, Nuba Mountains, Sudan.

1. INTRODUCTION

Uraniferous pegmatitic occurrences are widespread. Potassic pegmatites with uraniferous niobo-tantalates were reported from Antsirabe, Madagascar. In Sudan, Khor Anderachwan pegmatites, Red Sea hills, are composed of tourmaline and pyrite as the main ore minerals along with undifferentiated U- and Th-bearing minerals (Putzer 1956). Khalil (1980) has described five anomalies in the Nuba Mountains: Uro-Kurum; J. El Ugheibish, Lagawa; Miri, Kadugli; Katla, El Dilling; and J. Dumbeir, El Semeih. The uraniferous pegmatites of Miri Barra (present study) are thin short veins grading into quartz-rich stockworks and predominate at the contacts of Miri syenite batholith and its enclosing Precambrian Granitic gneisses basement.

Previous investigations on the distribution of radioactive hazards revealed very anomalous Rn activity in various sampling media along the zone of mineralization (Khalil

Nilo-Ethiopian Studies 1: 43–56 (1993)

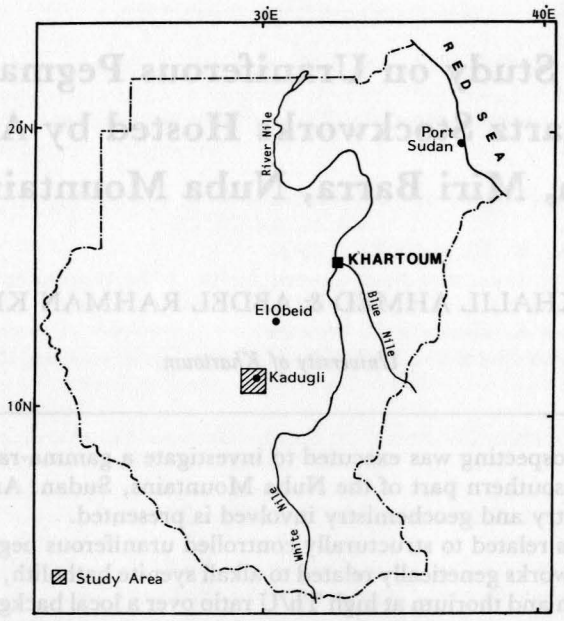

Fig.1. Location map of study area, Sudan.

1980; Uchdrof & Khalil 1985).

This study is confined to a limited part of the Miri anomaly (4.5 km^2), at the intersection of co-ordinates 11°5' and 29°34' 30", 20 km NW of Kadogli, Nuba Mountains (Fig.1). Investigations have included detailed geological mapping using aerial photographs at 1:12,000 scale, pertrographic studies, radiometric survey at 120 m × 50 m grid-system covered by GSP-1SL scintillometer and GAD-6 spectrometer with SP-4 sensor, and geochemical survey (using the same grid-system). The collected rock and mineralized samples were analyzed by neutron activation (U & Th only), fluorimetry (extractable U) and XRF. Elements analyzed and results are shown on the Appendix.

2. GEOTECTONIC SETTING

2.1. Regional geological and structural settings:

On a regional scale, Miri area is located in a terrain formed of basement rocks including Precambrian basement and younger anorogenic intrusive complexes.

The older basement is represented by granitic gneisses and schists. On the other hand, the post-orogenic intrusives are represented by the younger intrusive alkali complexes which extend in a northwesterly trending belt. This belt extends from Talodi to Lagawa (Tulishi), on the southwestern portion of the Nuba Mountains (Khalil 1986; Fig.2).

The Miri syenite batholith (Fig.3) is formed of alkali syenites, including subordinate quartz syenites and granites, minor gabbroic phases, diorite and granodiorte, and minor phases of pegmatitic syenite.

The dominant regional trend is the NNE foliation in the basement rocks. Block faulting is believed to control the emplacement of the intrusive complexes in a NNW-SSE belt (Khalil 1980). The region is dissected by approximately E-W, N-S and NNE transverse and wrench fault zones. Evidence of intensive deformation is represented by different patterns of folds which are recorded in the basement rocks (El Nadi 1980).

2.2. Geology of the lake Miri area

The major rock types at Miri (Fig.4) are alkali syenites. Considerable textural inhomogeneity is evident, particularly in the margin of the batholith (south of Miri dam),

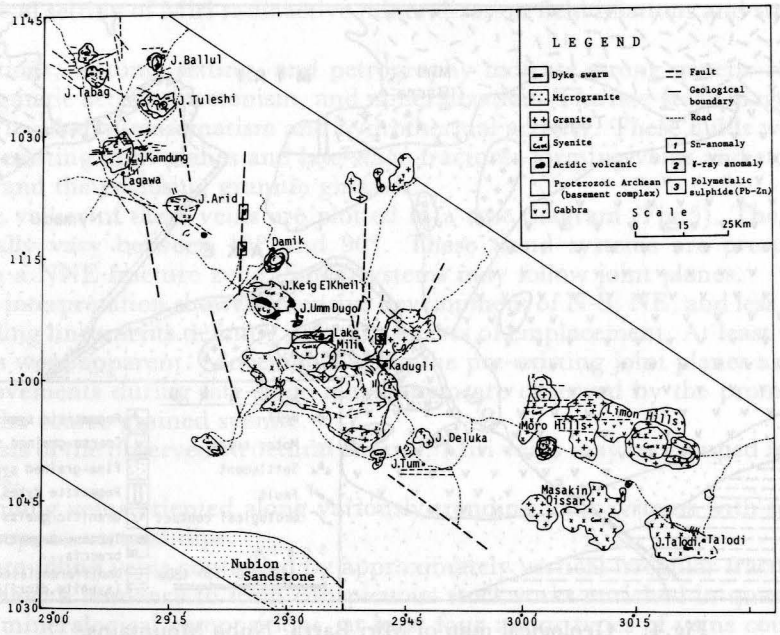

Fig.2. Geological map of Talodi-Lagawa belt, Nuba Mountains.

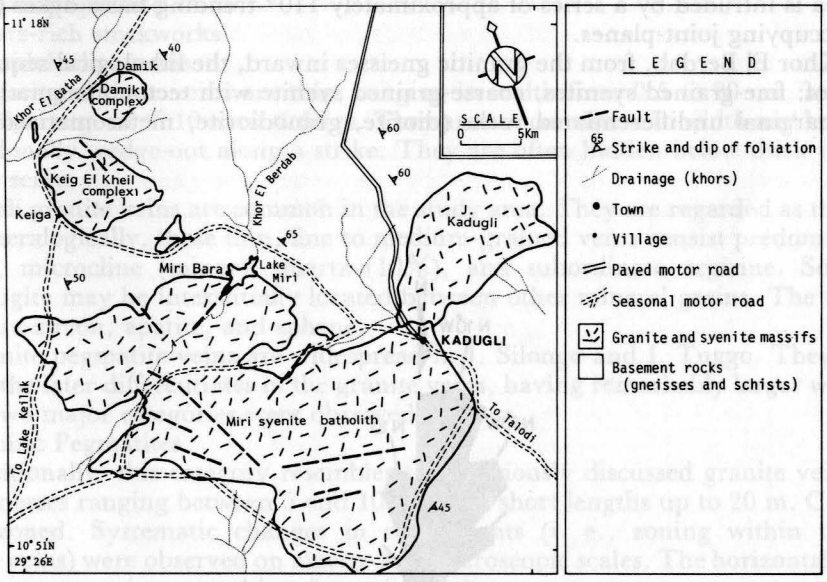

Fig.3. Geological map of lake Miri region, Nuba Mountains (After El Nadi 1980).

where lithological variations occur within a few meters. The lake site is located on part of a NNE fracture zone, which has high gamma ray and radon activities.

The area is dissected by a major fault that runs approximately N-S. Khor El Berdab flows in a southwest direction, occupying the fault zone.

The dominant rocks include syenites, diorites, and granodiorites. The syenites are generally fine to coarse-grained. The coarse-alkali syenite is xenolithic with the fine-grained variety, and in turn, is brecciated and metasomatized to form aegirine-rich tectonomagmatic breccia. This is weathered into boulders ($>$ 2 m across) well exposed at J.

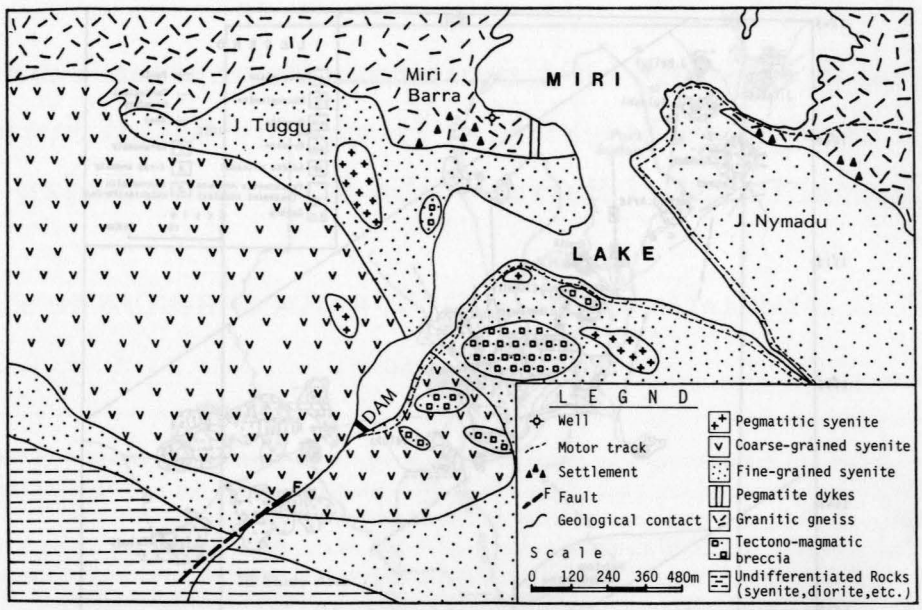

Fig.4. Geological map of Miri Barra, Nuba Mountains.

Silingo.

The area is intruded by a series of approximately 110° trending basic dykes (>30 cm across), occupying joint-planes.

Along Khor El Berdab, from the granitic gneisses inward, the lithological sequence is in the order of: fine-grained syenites, coarse-grained syenite with tectonomagmatic breccia, and the marginal undifferentiated rocks (diorite, granodiorite, metasomatized syenites, etc.).

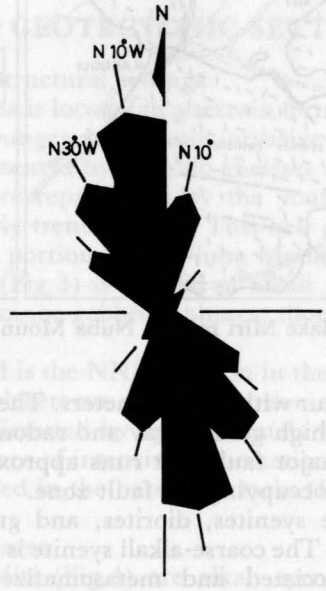

Fig.5. Rose diagram of the strikes of Miri radioactive veins.

2.3. Geological setting of Miri radioactive mineralization field relations and structural setting

Field relations, tectonic setting, and petrography indicate strong genetic relationships between magmatic activity, tectonism, and mineralization. The late-stage magmatic activity gave rise to alkali metasomatism and hydrothermal activity. These fluids were injected into the pre-existing joint planes and late-stage fractures forming veins and stockworks in the syenites and the enclosing granitic gneisses.

The strike values of these veins are plotted in a rose diagram (Fig.5). The dips of the veins generally vary between 15° and 90°. These trend systems are presumed to be developed in a NNE fracture zone. Some systems may follow joint planes.

Air-photo interpretation showed intensive development of N-S, NE, and less commonly, WNW trending lineaments defining different phases of emplacement. At least three major joint systems were apparent. Movements along the pre-existing joint planes are observed. Tectonic movements during late-stage magmatism are observed by the prominent NNE layering in the coarse-grained syenite.

On the basis of the observed structural control, Miri veins may be grouped into two major categories:

(a) Joint-filling veins oriented along variously trending joint systems with sub-horizontal, steep, to vertical dips.

(b) Fracture-filling veins controlled by approximately vertical irregular fractures. These veins have a tendency to form conspicuous stockworks enriched in quartz.

Based on mineralogical compositions, at least four major types of veins could be identifies in this respect:

(a) Alkali granite veins

(b) Granite pegmatite veins

(c) Quartz-rich stockworks

(d) Colloidal silica veins

The majority of these veins are thin, ranging in width from 0.5 to 20 cm, and having lengths in the range of $<$ 10 m to $<$ 50 m. They are not consistent in width and length, and may occasionally wedge-out along a strike. They are often hidden below thick vegetation and under scree.

The alkali granite veins are common in the study area. They are regarded as the earliest veins. Mineralogically, these thin, fine to medium-grained veins consist predominantly of orthoclase, microcline (minor), quartz (10%), and subordinate aegirine. Sometimes, aegirine-augite may be interstitially located between other mineral grains. The major accessories are zircon, apatite, and sphene.

The granite pegmatite veins are widespread in J. Silongo and J. Tuggo. They are considered as the later differentiates of the granite veins, having remarkably larger widths and lengths. Two major categories were observed.

(a) Granitic Pegmatites

Compositionally, this category resembles the previously discussed granite veins. They have thicknesses ranging between 5 and 10 cm, and short lengths up to 20 m. Commonly they are zoned. Systematic changes in constituents (i. e., zoning within individual pegmatitic veins) were observed on macro- and microscopic scales. The horizontal aspect of zoning is more prominent, and has five principlal components:

(1) Syenite wall-rock.

(2) An outer band of mafic minerals, mainly aegirine prisms, zoned spessartite, almandite, and a bright pink pleochroic isotropic mineral [uranothorianite (?)]

(3) An outer-intermediate band composed of predominantly of orthoclase, some microcline and quartz, which are riddled with small aegirine needles and zoned garnet.

(4) An inner-intermediate band containing a thin band of minute crystals of hornblende and garnet.

(5) A central zone (core) of medium-coarse grained pure quartz with some alkali feldspars (mainly ortho clase). Apatite forms needles and prisms which are enclosed

in the quartz and feldspars.

(b) Quartz-aegirine-bearing pegmatites

Very coarse-grained quartz-aegirine-bearing pegmatites are locally observed (J. Silingo) as veins cutting into the coarse-grained alkali syenites and the associated tectonomagmatic breccia. These veins are fracture fillings and exhibit a distinct fabric, as opposed to granitic composition. They generally fill vertical fractures, with strikes of NNE, 106°, 210° and NNW, traceable over short distances. The maximum observed width in rarely above 20 cm.

In thin sections, these veins are mainly composed of aegirine (about 70%), quartz (25%), and subordinate orthoclase (<5%). Among the accessories, zircon and iron ore are common, while apatite and fluorite are less common. Aegirine is well crystallized forming well-developed columnar crystals up to > 5 cm long and is characterized by shiny black color. Crystals are grown and arranged with their parallel axes vertical to the walls of the veins.

3. RESULTS OF DETAILED SURVEYS IN MIRI AREA

3.1. Radiometric survey

Gamma ray measurements (spectrometric and scintillometric) were conducted in the region that encompasses Miri syenite batholith (Fig.6) and the western portion of Kadogli, with detailed radiometric mapping around Lake Miri. Significant anomalous gamma-ray counts were measured during the survey.

The anomalies could be followed over horizontal distances along a major NNE fracture-zone, which crosses the batholith and extends beyond the superficial cover to the western peripheries of Kadogli. Scintillation counts were recorded over syenites, quartz-syenites, gneisses, and in places over superficial sandyclayey material.

Radiometric mapping around Lake Miri in an area of approximately 3 km^2 (Fig.7) was carried out at 1:2,000 scale and on a 150 m × 50 m grid, with ten N-S profiles.

The highest counts cover a range between 900 and 3000 CPS. These were measured in the late-stage pegmatitic and quartz-rich veins. The inhomogeneity of the U and Th distribution within these veins is reflected by the variation in gamma-ray counts of these two elements. The anomaly is open, indicating a broad zone of mineralization, and is

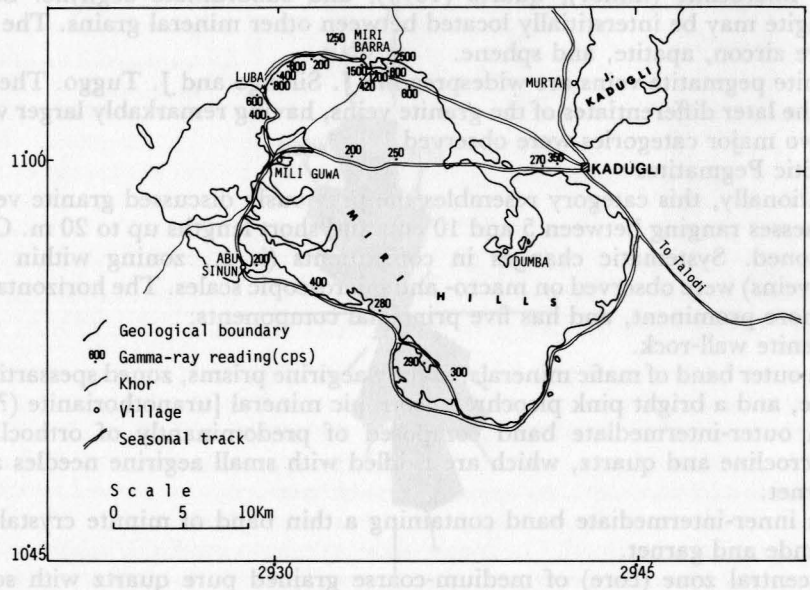

Fig.6. Gamma-ray measurements over Miri complex, Nuba Mountains.

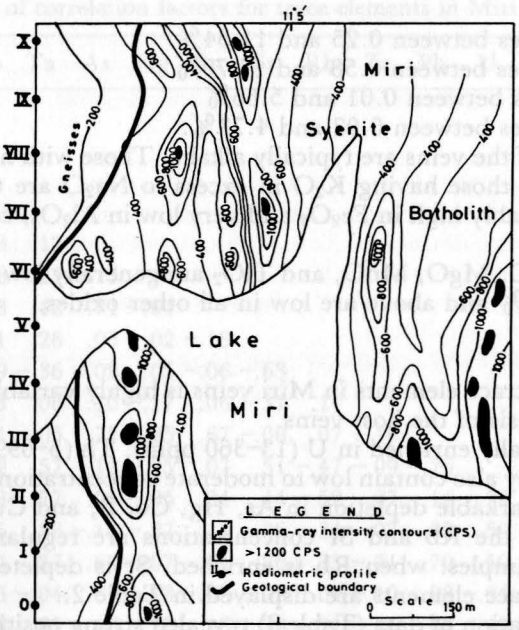

Fig.7. Radiometric map, Miri area.

oriented in approximately an E-W direction. The survey area is generally covered by low count-rates (values over 500 CPS), cover more than 20% of the survey area.

It became evident that radioactive hazards are distributed in the water (Uchdrof & Khalil 1985), soil, rocks, and air of the Miri area. These are represented by hazards due to radioelements U^{238}, Rn^{222} and possibly Rn^{220}. In addition, a variety of toxic elements, As, Se, Hg, etc., were recorded in blue and brown algal-rich soil samples in the vicinity of the spring along Khor El Berdab (Fig.4).

3.2. Geochemistry of Miri radioactive Veins:P

3.2.1. Major elements

Miri radioactive elements-bearing veins (Table 1) are highly siliceous, with SiO_2 ranging between 61.60 and 95.53%. The major element oxides of Al, Fe, Na, and K, are strikingly

Table 1. Major elements in Miri radioactive veins (%)

	SiO_2	TiO_2	Al_2O_3	Fe_2O_3	MnO	MgO	CaO	Na_2O	K_2O	P_2O_5
Aegirine-rich vein	70.17	0.33	0.48	10.19	0.14	0.51	1.06	3.34	2.37	0.63
M20	74.60	0.44	0.44	9.48	0.31	0.52	0.55	1.51	2.34	1.19
Quartz stockwork	90.00	0.66	0.65	3.20	0.10	0.51	0.47	0.00	0.82	0.50
Quartz stockwork	73.56	0.37	0.84	8.33	0.13	0.62	0.49	2.89	3.38	0.98
Quartz stockwork	75.08	0.44	0.93	8.78	0.13	0.68	1.76	2.78	2.64	0.66
Quartz stockwork	83.99	0.35	0.50	5.00	0.22	0.65	0.44	0.99	2.68	1.41
M25-1	74.71	0.40	4.61	6.17	0.93	0.06	0.46	2.48	2.46	0.72
M25-2	87.59	0.08	3.93	0.81	0.23	0.03	0.16	0.18	2.45	0.53
Aegirine-rich vein	62.35	0.91	6.62	17.70	0.16	0.18	0.85	3.23	3.64	0.28
Granite vein	63.25	0.04	9.30	8.81	0.06	0.17	0.16	2.40	3.97	0.61
Granite pegmatite	61.60	0.72	11.54	10.36	0.67	0.23	0.72	4.82	4.73	0.16
Quartz stockworks	91.06	0.68	0.25	3.20	0.10	0.51	0.47	0.02	0.82	0.53

variable:

Al_2O_3 varies between 0.25 and 11.54%
Fe_2O_3 varies between 0.58 and 17.70%
K_2O varies between 0.01 and 5.66%
Na_2O varies between 0.02 and 4.73%.

The vast majority of the veins are typically alkalic. Those with high Na_2O over K_2O are termed "sodic," while those having K_2O in excess to Na_2O are termed "potassic." The sodic veins are remarkably high in Fe_2O_3 and very low in Al_2O_3, compared to the potassic veins.

The contents of CaO, MgO, MnO, and TiO_2 are generally low in both categories. The veins with silica of 90% and above are low in all other oxides.

3.2.2. Trace elements

The distribution of trace elements in Miri veins is highly variable. This could be due to the differences in genesis of the host veins.

The veins are generally enriched in U (13–360 ppm), Th (5–699 ppm), Zr, Nb, Ta, Y, Sr, REE, and Rb. They also contain low to moderate concentrations of Ba, Ga, W, Sn, Hf, Pb, and Be, with remarkable depletion in As, Hg, Co, B, and Cu.

It is indicated that the Rb and Sr concentrations are regularly and antipathetically distributed in most samples: when Rb is enriched, Sr is depleted, and vice-versa. The averages of selected trace elements are displayed in Table 2.

Computer Interpretation of data (Table 3) revealed strong positive correlations between Pb-Sn-As-Yb-La and U-Th-Sr-Hf-Ta-Ce-Gd. Weak positive correlations exist between U-Th and Sr-Nb. On the other hand, slightly stronger negative correlation exists between Rb and Sr ($r=0.47$). Other correlations are shown on Table 3.

The above significant correlations could be useful in delineating different mineral phases and associations. The light REE (Ce and La) and the heavy REE (Yb and Gd) displayed a remarkable geochemical affinity to U and Th at different levels. It seems likely that precipitation of the REE started with a low La/Yb ratio (i. e., La < Yb) and progressively increased as mineralization proceeded, with Yb becoming diminished and La and Ce enriched. This may have lead to the precipitation of La and Ce with U at a relatively medium La/Ce ratio. As Th is enriched, Gd is enriched and precipitated with Th at lower

Table 2. Selected trace elements in 19 mineralized vein samples, Miri area (ppm).

	Mean	Minimum	Maximum
U	122.3	13	300
Th	183.0	5	769
Zr	11,381.5	310	58,709
Nb	4,017.2	275	9,544
Ta	214.8	16	1,200
Pb	267.8	13	982
Sn	158.1	9	479
Zn	191.4	15	798
Ni	213.5	8	2,611
Ba	555.3	100	2,000
Be	208.0	3	3,000
Sr	541.1	9	1,811
Y	1,160.7	156	2,226
Ce	5,168.4	100	50,000
La	1,092.1	50	3,000
Rb	259.4	36	477

Table 3. Computation of correlation factors for trace elements in Miri veins (n=19 samples).

	Mo	W	Hf	Nb	Ta	As	Hg	Sn	Sr	Rb	Zr	Pb	U	Th	Ce	La	Yb	Gd
W	−.14																	
Hf	−.38	.09																
Nb	.06	.08	−.27															
Ta	−.12	−.04	.68	.39														
As	−.11	.02	−.20	−.23	.13													
Hg	−.31	.01	.15	.36	.21	.13												
Sn	−.05	.03	.12	−.03	.12	.71	−.01											
Sr	−.21	−.29	.27	.11	.26	.06	.02	−.18										
Rb	.16	.13	−.36	−.09	−.36	−.09	.05	−.06	−.63									
Zr	.44	.21	−.01	−.03	.06	.10	−.17	.06	−.31	.14								
Pb	−.17	−.09	−.10	−.21	−.05	.73	.25	.67	−.08	.07	−.16							
U	−.23	.11	.58	.32	.57	.12	−.25	.07	.51	−.47	−.09	−.20						
Th	−.24	.05	.75	.13	.77	.05	−.05	.04	.44	−.52	.07	−.14	.79					
Ce	−.21	.14	.81	.16	.88	−.11	−.27	.11	.36	−.34	.07	−.08	.59	.69				
La	−.37	.15	.39	.04	.37	.64	−.07	.61	.26	−.33	−.21	.70	.50	.38	.42			
Yb	−.16	−.06	−.08	−.16	−.04	.67	.23	.68	−.09	.04	−.10	.98	−.24	−.16	−.10	.66		
Gd	−.26	−.17	.83	.16	.85	−.16	−.20	.16	.29	−.31	−.16	.02	.49	.55	.96	.45	.10	

Table 4. Comparison of total with extractable uranium (in ppm).

Sample No.		Total uranium TU (XRF)	Extractable uranium EU (fluorimetry)	Ratio EU/TU	% EU/TU
1	M1	174	24.0	0.138	13.8
2	M3	30	4.5	0.158	15.8
3	M5	82	13.3	0.162	16.2
4	M7	750	149.0	0.199	19.9
5	M8	238	40.7	0.171	17.1
6	M10	61	13.1	0.215	21.5
7	M11	163	20.2	0.124	12.4
8	M13	186	32.1	0.173	17.3
9	M20	33	6.3	0.191	19.1
10	M25.1	141	27.0	0.191	19.1
11	M25.2	210	30.0	0.143	14.3
12	M	132	12.9	0.098	9.8
13	M31	25	4.6	0.184	18.4
14	M32	296	71.2	0.241	24.1
(X)*		180.14	26.35	0.162	16.2
(S)		177.63	37.16	0.139	
(C.V.)		98.61%	141.02%	85.80%	
(N)		14	14	14	

* X=mean, S=standard deviation, C.V.=coefficient of variation, and N=number of samples.

Ce/Gd ratio (i. e., Ce < Gd). This is suggested by the positive correlations of Ce and La with U; Ce and Gd with Th; Ce with Gd (0.96); and La with Yb.

Computation of the ratio of extractable U(E)/total U(T) gave an average content of 16% (Table 4). This may show the tendency of uranium to form separate uranium mineral phases.

3.3. Implications of the chemistry of mineralizing solutions

The high alkalinity of the original magma from which Miri syenites were formed enabled U and similar transition elements to form stable complexes. Thus, they were not incorporated into the lattices of normal silicate minerals, but concentrated in the final products of the magma (late pegmatitic melt/late hydrothermal fluids), through formation of alkali, fluoride, and phosphate complexing.

The original mineralizing solutions were presumably alkali granite melts and pneumatolytic fluids (high temperature solutions) that accumulated in the late stages of strong acidic phase(s). These solutions carried U, Th, Zr, W, Sn, Mo, Ta, and Bi partly in fluoride and sulphur phases to form pegmatitic veins. The presence of high Rb and low Se indicates partial formation from a magmatic melt. The late-stage solutions were typically medium to low temperature hydrothermal fluids. However, the earliest phases may represent late pegmatitic/hydrothermal interaction at relatively higher temperatures. The important elements carried by these fluids include: U, Th, REE, Hf, Y, Sr, Zn, Cu, Ni, Pb, and may include some Nb, Ta, and Sn, which are stable over a wide range of pH and P-T conditions.

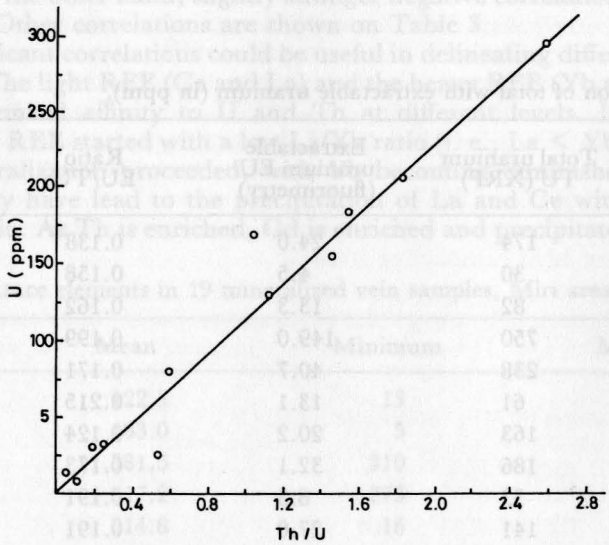

Fig.8. Plot of U versus Th/U for Miri radioactive veins.

The strong positive correlation between Th and Th/U ration is indicated by the coherency of U and Th distribution (Fig.8), signifying formation from a primary solution at high temperatures. Uranium and thorium were primarily incorporated in complexes as U^{4+} and Th^{4+} (i. e., reduced forms), respectively.

Soviet studies of U deposits have indicated that the formation of uraninite occurs above 150 C° whereas pitchblende (massive, microcrystalline and colloform variety of uraninite) forms at temperatures not exceeding 220 C° and probably less than 200 C° (Naumov 1959). Due to the lack of any data on fluid inclusions and isotope analysis, the temperature of mineralization was not predicted in this work.

3.4. Mineralogical sites of uranium and other trace elements

Because of insufficient data on mineralogy and petrology, the mineralogical site of uranium and the accompanying elements is poorly understood. However, the mineral distribution of the different trace elements assemblages in Miri could be ellucidated as follows:

(1) The high REE contents, especially the light rare earth elements (Ce and La), are likely to be present in separate rare earth minerals, e. g., bastnaesite. Some of these may be incorporated in uranium minerals and refractory mineral phases.

(2) Tthe low Sn and W may occur as minor disseminations of cassiterite and wolframite, but to some extent could be held in other minerals, e. g., zircon, aegirine, etc.

(3) The high contents of Nb and Ta may be hosted by co lumbite-tantalite (such as betafite, devidite, etc.), or at least may be hosted by the REE and uranium minerals.

(4) The observed uranium- and thorium-bearing minerals include monazite, apatite, aegirine, zircon, sphene, and allanite. In addition, other possible minerals may include euxenite and thorite; the maximum uranium oxide contents (as quoted in literature) in the lattice of these minerals are 20% and 12%, respectively. The presence of uranium-bearing mineral phases (other than the refractory minerals) could be confirmed by the slightly higher extractable U/total U ratio (averages 16%). The U-Th bearing minerals may carry considerable contents of Hf, REE, Sr, Y, and some Pb.

(5) A late stage of minor sulphide mineralization includes minerals of As, Mo, Ph, Zn, Cu, and Ni.

4. CONCLUSIONS

(1) Uranium mineralization of Miri is related to late-stage magmatic pegmatite veins and hydrothermally formed quartz-rich stockwork; all being related to Miri syenite batholith. Multi-phase mineralization with a group of incompatible elements is evident.

(2) Thorium, Hf, REE, Ta, Nb and Sr can be used as pathfinders in geochemical prospecting for uranium-thorium mineralization in anorogenic syentitic complexes, especially when pegmatites are encountered.

(3) Further explorational work is needed in the study area to reveal the potentiality of U and Th or other elements.

(4) The environmental impact of mineralization has to be adequately studies, since radioactive hazards of U and Th and their daughter products, as well as a number of toxic elements, were detected at high concentrations in variable sampling media.

ACKNOWLEDGMENTS

Most of analytical work was sponsored by the IAEA. The authors gratefully acknowledge the considerable help of Prof. G. R. Parslow, Univ. of Regina, Canada, and Dr. Farouk Happani, Univ. of Khartoum during analysis. Thanks are due to Mahmoud S. Ahmed for preparing final drafts of maps and Salih A. Salih for typing the manuscript.

REFERENCES

El Nadi, A. H.
1980 *The Geology of Keig El Khali, Damik and Umm Dugo Igneous Complexes, Nuba Mountains, Sudan.* Unpublished MSc. Thesis, Univ. of Khartoum, Khartoum, Sudan.

Khalil, B.
1980 Geology and prospecting for mineral deposits in the Precambrian Basement complex of the Nuba Mountains, Sudan 6th Conf. Ged. Soc. of Africa, Nairobi: 23 pp.

1986 Preliminary confidential report on unclear hazards due to uranium-thorium mineralization, Miri Lake, Kadogli area, Nuba Mountains, Sudan, [unpub.].

Naumov, G. B.

1959 Transportation of uranium in hydrothermal solutions as carbonate complexing. Geochem., pp: 5–20.

Putzer, H.

1956 Report on the occurrence of radioactive minerals at Khor Inderaikwan, Red Sea Province, Sudan [unpub.]

Uchdrof & B. Khalil

1985 Radon and gamma-ray measurements in the Nuba Mountains, Sudan [unpub.].

BADR EL DIN KHALIL AHMED: *University of Khartoum, P. O. Box 321, Khartoum, Sudan*
ABDEL RAHMAN KHIDER HASSAN: *University of Khartoum, P. O. Box 321, Khartoum, Sudan*

Appendix 1. Trace element contents in radioactive veins (in ppm).

	(1) M1	(2) M2	(3) M3	(4) M5	(5) M7	(6) M8	(7) M9	(8) M10	(9) M11	(10) M12	(11) M13	(12) M14	(13) M16	(14) M19	(15) M20	(16) M25-1	(17) M25-2	(18) M26	(19) M30
Ni	47	309	8	65	15	—	30	199	29	89	498	38	31	—	68	19	2611	16	—
Co	—	3	—	20	3	10	—	—	3	35	16	3	8	74	—	9	—	3	—
Mo	21	87	98	58	—	5	8	155	19	4	22	9	16	8	—	13	13	5	93
W	33	5	16	83	18	—	29	9	12	38	28	27	114	315	114	—	19	30	139
Hf	—	8	13	3	105	24	61	3	4	21	—	6	62	21	21	—	16	—	14
Nb	8906	1101	1822	2859	5112	498	8866	9447	922	5729	1323	1271	5310	275	9544	2642	3912	3741	3046
Ta	210	28	51	77	1200	116	289	366	36	150	16	153	554	37	220	29	211	88	250
Cu	—	19	28	—	6	—	2	3	12	215	12	17	—	11	3	3	15	17	60
Zn	98	25	83	169	58	191	68	286	79	306	15	207	231	136	133	277	798	413	63
As	16	—	25	28	—	3	—	21	39	5	—	141	61	28	20	119	27	—	39
Hg	10	3	—	—	2	15	—	—	27	16	28	18	16	6	—	—	8	—	3
Bi	4	—	—	—	8	3	29	—	—	14	3	9	13	—	—	3	17	—	30
Sn	100	14	183	100	200	100	190	210	196	11	9	479	150	300	250	261	22	28	200
Ga	49	—	65	105	93	89	114	35	50	—	—	200	69	56	98	100	30	30	50
Ba	300	2000	100	300	1000	100	1000	300	100	1000	100	1000	650	100	100	1000	300	100	1000
Be	100	10	30	50	100	50	100	50	50	20	3	100	30	30	50	50	30	3000	100
Sr	56	1811	61	112	1316	1003	1113	112	112	88	696	347	1112	236	180	1312	307	298	9
Y	2226	156	962	664	1110	403	2006	3515	301	1319	123	1313	2690	333	410	499	922	1101	2000
Rb	447	107	477	662	47	36	53	349	253	670	263	317	47	366	256	111	232	198	37
Zr	43648	343	13432	9811	3115	9998	2637	13291	3101	9931	606	10312	15000	758	3337	11211	5121	1825	58709
Pb	138	13	230	318	237	312	598	100	318	27	19	982	351	188	91	866	118	47	102
B	10	100	3	—	—	3	10	30	10	30	200	10	—	30	—	10	100	10	23
U	170	21	30	80	300	162	239	186	61	25	31	19	296	104	33	309	210	32	116
Th	130	36	5	45	699	299	151	204	7	11	89	195	769	160	6	295	159	101	1000
Ce	1000	1000	1000	1500	150000	1000	10000	3000	1000	100	300	500	7500	1000	500	10000	3000	3000	300
La	1000	100	300	300	3000	1000	300	1000	500	—	50	1000	2000	1000	200	3000	2000	1000	150
Yb	100	10	100	—	50	100	100	30	10	50	20	30	50	50	100	50	30	30	100
Gd	10	—	10	—	300	10	100	—	30	—	10	10	10	—	10	10	30	—	—

M1 Alkali granite vein
M2 〃 〃 〃
M3 〃 〃 〃
M5 Quartz-rich stockworks
M7 Quartz-rich stockwork
M8 Granite pegmatite vein
M9 〃 〃 〃
M10 Very coarse-grained aegirine bearing pegmatite
M11 Aegirine-rich pegmatites
M12 Granitic pegmatite vein
M13 Fine-grained syenite
M14 Granite vein
M16 Quartz-rich stockworks
M19 granite pegmatite
M20 Quartz-aegrine-bearing pegmatite
M25–1 Quartz-rich stockworks
M25–2 Quartz-rich stockworks
M26 Pegmatite vein
M30 Quartz-rich stockwork

Appendix 2. Activation analysis of samples from Miri area.

Sample	U (ppm)	Th (ppm)
course-grained syenite	7	13
coarse-grained syenite	8	26
fine-grained syenite	5	13
fine-grained syenite	10	17
pegmatitic syenite	12	40
basic dyke	8	14
basic dyke	136	460
quartz-rich stockwork	199	880
quartz-rich stockwork	96	550
quartz-rich stockwork	136	460
quartz-rich stockwork	50	230
quartz-rich stockwork	140	630
granite pegmatite	61	1
granite pegmatite	34	22
granite pegmatite	43	50
granite pegmatite	34	22
aegirine-rich vein	35	43
aegirine-rich vein	10	55
aegirine-rich vein	67	<1
M2	29	36
M3	1	43
M7	156	270
M10	231	107
M11	51	3
M14	36	27
M16	199	880
M20	37	1
M25–1	324	460